Supporting Information for

Polycrystalline Fe- and Sn-based Sulfides for High-Capacity Sodium-Ion Battery Anode

Xinxin Zhu, Peng Wang, Yihong Ding*, Ying Chu, Jie Lin, Shiqiang Zhao*, Huile Jin and Tianbiao Zeng*

Key Laboratory of Carbon Materials of Zhejiang Province, Wenzhou Key Lab of Advanced Energy Storage and Conversion, Zhejiang Province Key Lab of Leather Engineering, College of Chemistry and Materials Engineering, Wenzhou University, Wenzhou Zhejiang 325035, China.

*: Corresponding authors. Email: yhdd@wzu.edu.cn; zhaosq@zju.edu.cn ; yhdd@wzu.edu.cn

1. Experimental

1.1 Synthesis of materials

Chemical analytical purity of SnS_2 powder, Fe powder, FeS powder, SnS_2 powder, and graphite powder was supplied from Shanghai Aladdin Reagent Co., Ltd., and used wither further treatment. Typically, 8.0 mmol Fe powder and 16.0 mmol SnS_2 powder were mixed and loaded into a quartz tube of 10.0 cm length, 1.0 cm outer diameter, and 1.0 mm thickness. The tube was evacuated until the pressure was less than 10 Pa, then seal and heated in muffle a furnace at 600 ℃ for 2 days with a temperature raising slop of 5℃ min^{-1}. After heating finished and the temperature was cooling down to room temperature spontaneously, polymetallic sulfides powder was obtained (denoted to FSS). Next, the as-prepared powder was mixed with graphite powder in the mass ratio of 95:5, 85:15, and 75:25 and loaded into a 50 mL N_2-filled stainless steel ball mill, then rotate 6 h at 800 rpm. After the ball milled finished, polymetallic sulfides anchored on exfoliated graphite were obtained (denoted to FSS/G-5%, FSS/G-15%, and FSS/G-25%, respectively).

The 15 wt.% exfoliated graphite containing nano FeS anchored on exfoliated graphite was prepared by ball milling commercial FeS with commercial graphite, the ball milling protocol was the same with the preparation of FSS/G-15%. The obtained sample denoted to FeS/G-15%. The 15 wt.% exfoliated graphite containing nano SnS_2 anchored on exfoliated graphite was prepared in the same method, and the sample was denoted to SnS_2/G-15%. The Sn_2S_3 powder was prepared by following strategy: Sn powder and S powder were mixed in a 2:3 mole ratio, then 0.500 g mixed powder was loaded into quartz of 10 cm length, 1.0 cm outer diameter, 1.0 mm thickness, and evacuated until the pressure less than 10 Pa. The tube was heated at 350 ℃ for 24 h, then heated at 450 ℃ for 24 h, and the temperature increase slope was 1℃ min^{-1}. After heating finished and the temperature cooled down to room temperature, the tube was unsealed, and obtained powder was ball milling with 15 wt.% graphite in the same protocol was same with the preparation of the FSS/G-15%, the target product denoted to Sn_2S_3/G-15%.

1.2 Characterization

The crystal phase of samples was tested by Shimadzu-XRD-7000 XRD instrument (CuK_α, λ=1.54056 Å, 40 KV, 40 mA). The element state of FSS and FSS/G-15% were analyzed by X-ray photoelectron spectroscopy (XPS) (Axis Ultra DLD, USA). Morphology was acquired in FEI structure field emission scanning electron microscopy (FESEM, America) and Tecnai FEI transmission electron microscopy (TEM, America), and elements distribution of samples was studied in the same TEM.

All samples were mixed with acetylene black and sodium carboxymethyl cellulose with a weight ratio of 8:1:1, followed by adding a small amount of deionized water and stir 2 h to form a slurry, then cast the slurry on Cu foil, respectively. After drying, the foils were punched into 12 mm discs for electrodes, and the mass loading of samples was controlled to 1.5±0.2 mg cm^{-2}. CR-2032 coin cells were assembled in an Ar-filled glove box, and the water and oxygen of the glove box were lower than 0.5 ppm and 1 ppm. The electrolyte was 1 mol L^{-1} $NaFP_6$ contained in ethylene carbonate/dimethyl carbonate/propylene carbonate (1:1:1 in volume ratio) with 5 wt.%

fluoroethylene additive and separator was glass fiber membranes. Cyclic voltammetry and electrochemical impedance spectroscopy (EIS) tests were performed on CHI660E electrochemical workstation, and discharge/charge and galvanostatic intermittent titration technique (GITT) were tested on a LAND battery tester. The capacity was calculated based on the total mass of Sn_2S_3/Sn_3S_4/FeS/Fe_7S_8.

1.3 Theoretical calculation

First principles calculation (DFT) and molecular dynamics (MD) simulation were performed on the VASP package. Standard crystal files were downloaded from the materials project website. All structures were structurally optimized until the electronic self-consistency convergence to 0.01 meV/cell and 0.1 eV/Å. Cutoff energy was set to 520 eV. The K-point mesh was set according to <*a*>, <*b*>, <*c*>, which are integer parts of the *a*, *b*, and *c* parameters of the crystals. A generalized gradient approximation function of the Perdew-Burke-Ernzerhof correlation (GGA-PBE) was used to establish the exchange-correlation function. In Na^+ diffuse and work function calculation, the structures were constructed based on the standard crystal structure. The Na^+ diffuse coefficient was calculated based on the following equation[1, 2]:

$$D_{Na+} = \lim_{t\to\infty} \frac{< r^2(t) >}{6dt}$$

Where $<r^2(t)>/t$ is the slope of Na diffuse square displacement (MSD). The work function was calculated based on the following equation[3, 4]:

$$E_w = E_v - E_F$$

Where E_v is the surface vacuum energy level of an electronic in a given structure, E_F is the Fermi level of a given structure.

Figures

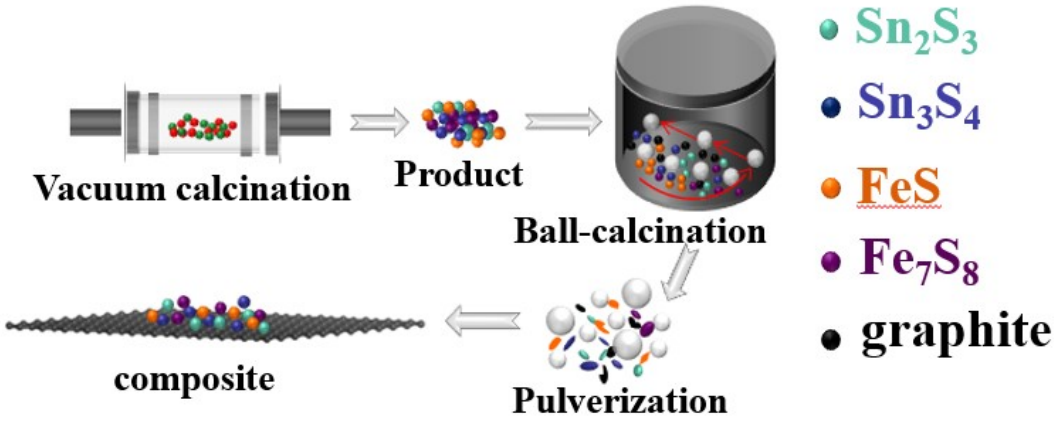

Fig. S1 Schematic synthesis process of FSS/G-*x*% (*x*=5%, 15%, 25%).

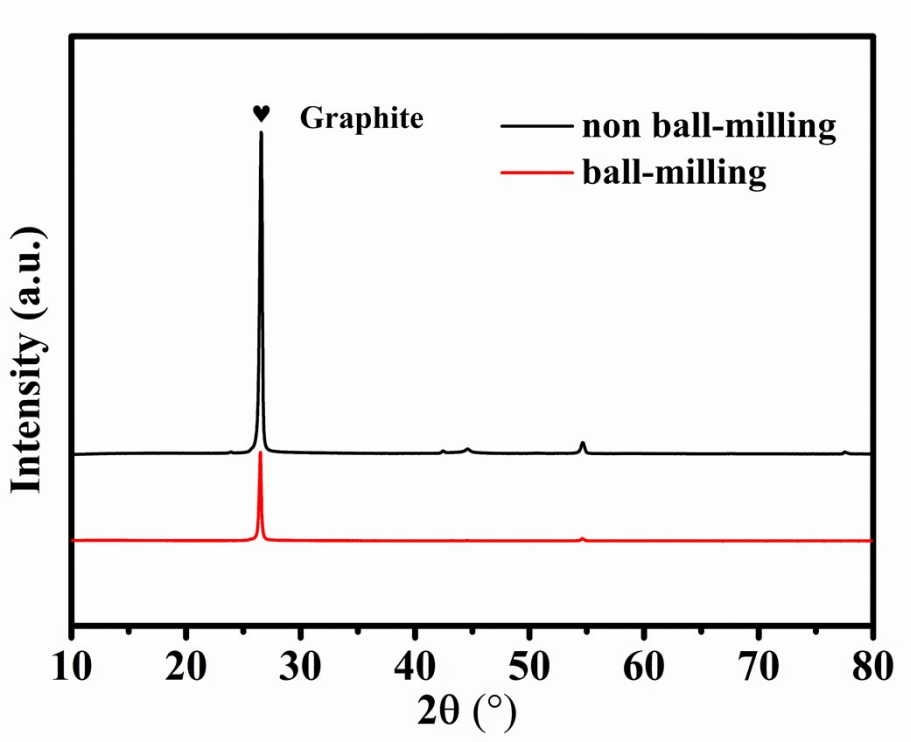

Fig. S2 XRD curves of graphite.

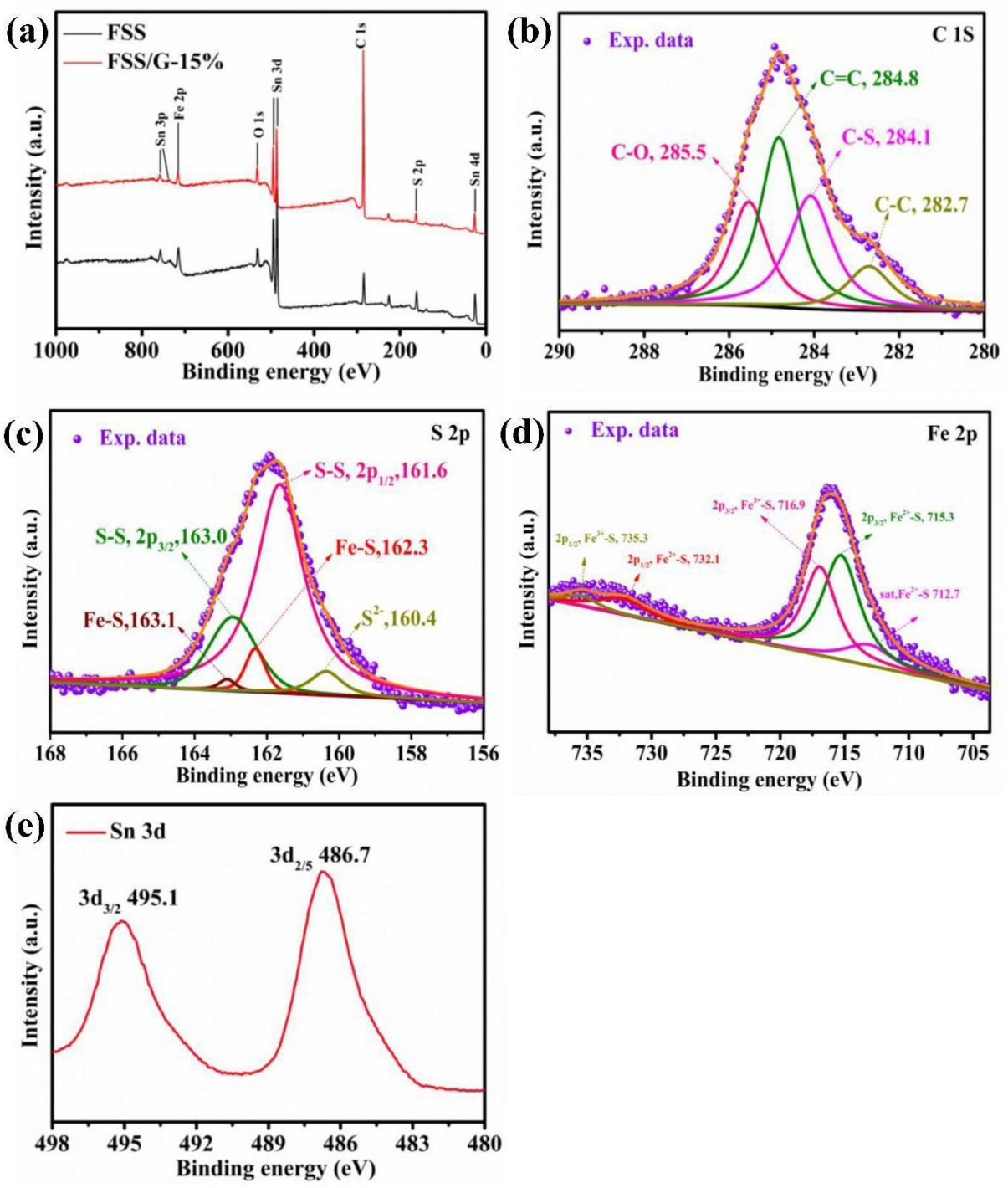

Fig. S3 XPS curves of FSS and FSS/G-15%. (a) Survey curvy, (b) C1s spectra of FSS/G-15%, (c) S 2p spectra of FSS/G-15%, (d) Fe 2p spectra of FSS/G-15%, (e) Sn 3d spectra of FSS/G-15%.

The surface chemical state of FSS and FSS/G-15% was revealed by the XPS test. The survey spectra (Fig. S3a) detected Sn, Fe, O, C, and S elements. Usually, the O element originated from the adsorbed

trace of H_2O and CO_2[5]. The C1s spectra of FSS/G-15% can be fitted to four peaks located at 282.7, 284.1, 284.8, and 285.5 eV, corresponding to C-C, C-S, C-C, and C-O bonds (Fig. S3b)[6]. In the situation of S2p spectra (Fig. S3c), five characteristic peaks can be fitted including 160.4, 162.3, 161.6, 163.0, and 163.1 eV, respectively, are the sp2 hybridization of S^{2-}, $2p_{1/2}$ of Fe-S, $2p_{1/2}$ of S-S, $2p_{3/2}$ of S-S, and $2p_{3/2}$ of Fe-S bonds[6, 7]. The Fe 2p spectra can be fitted to five peaks including 712.7, 715.3, 716.9, 732.1, and 735.3 eV, which are satellite peaks of Fe^{2+}-S, $2p_{3/2}$ of Fe^{2+}-S, $2p_{3/2}$ of Fe^{3+}-S, $2p_{1/2}$ of Fe^{2+}-S and $2p_{1/2}$ of Fe^{3+}-S, respectively (Fig. S3d)[6-9]. Sn 3d spectra show two classical splitting peaks located at 486.7 and 495.1 eV, and shift to lower binding energy compared to Sn_2S_3, indicating the presence of Sn^{3+} and $Sn^{8/3+}$ (Fig. S3e)[10-13]. Besides the C, O, Sn, S, and Fe peaks, no other impurity peaks are detected, illustrating the success of preparing polymetallic sulfides by using Fe and SnS_2 as starting materials.

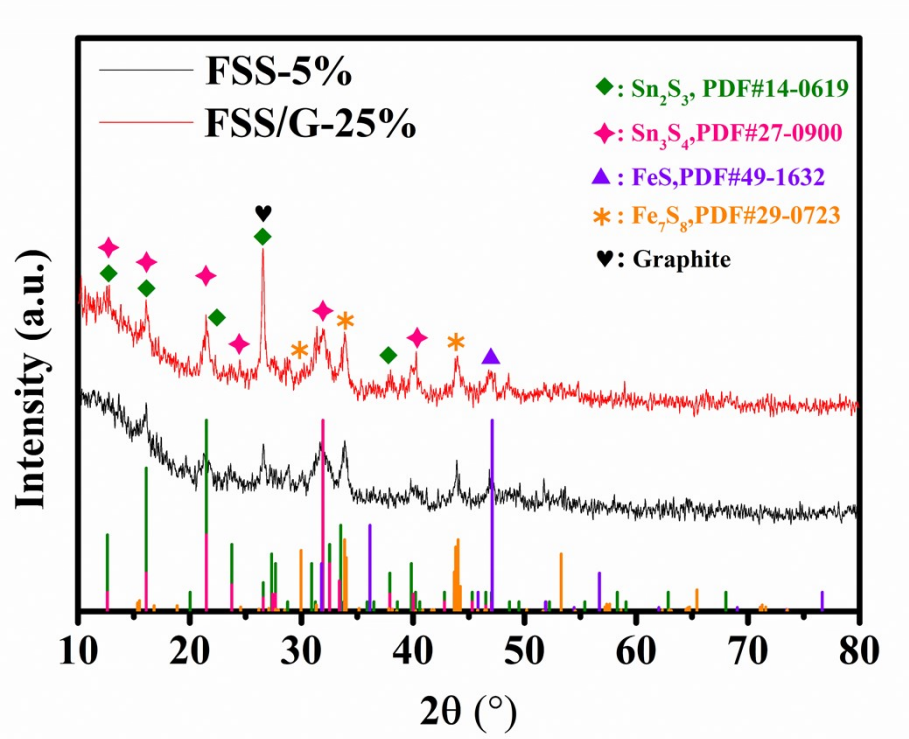

Fig. S4 XRD curves of FSS/G-5% and FSS/G-25%.

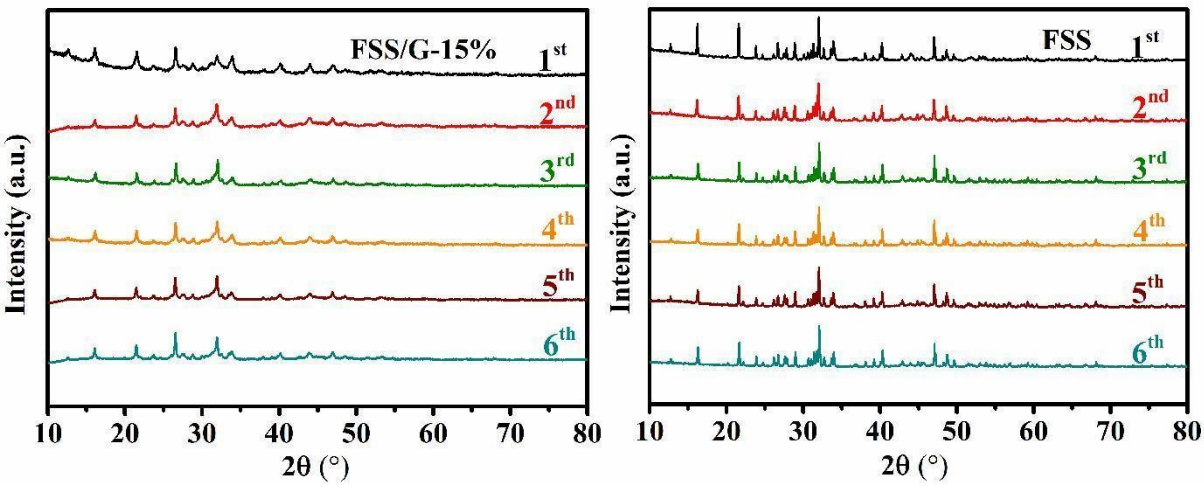

Fig. S5 XRD curves of repetitively synthesized samples. (a) bulk FSS, (b) FSS/G-15%. The 1st is the same as the XRD data of Fig. 2 in the main text, the 2nd ~ 6th are five repeated experiments.

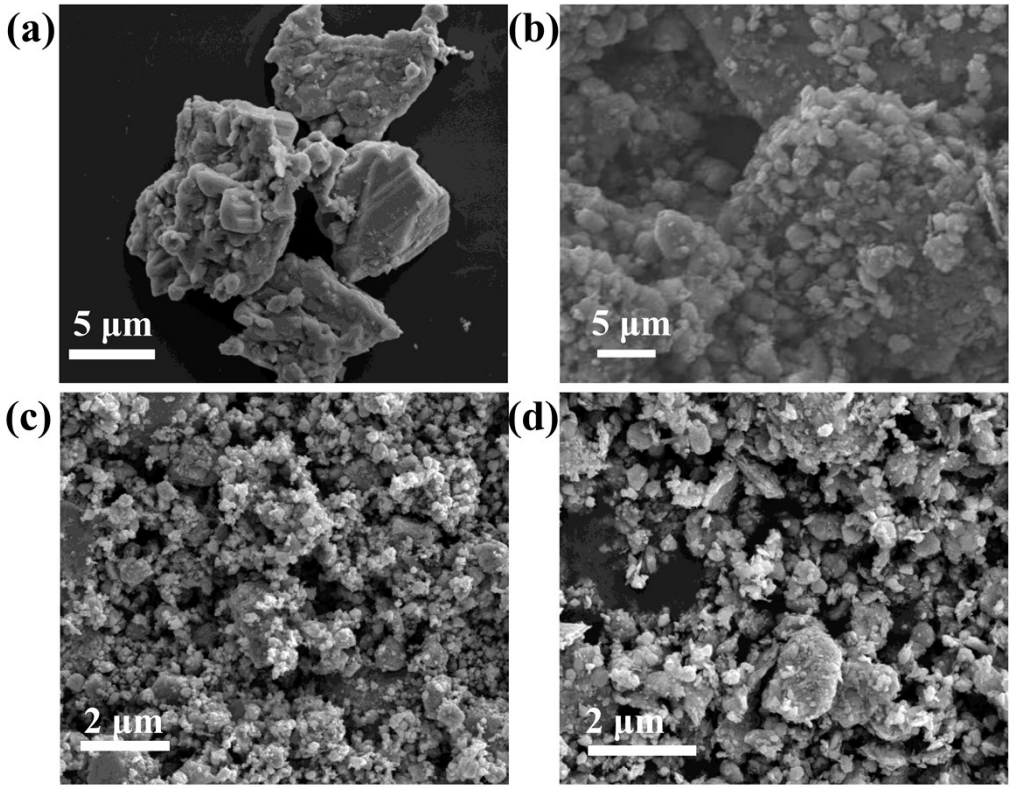

Fig. S6 SEM image of FSS (a), FSS/G-15% (b)， FSS/G-5% (c), FSS/G-5% (d).

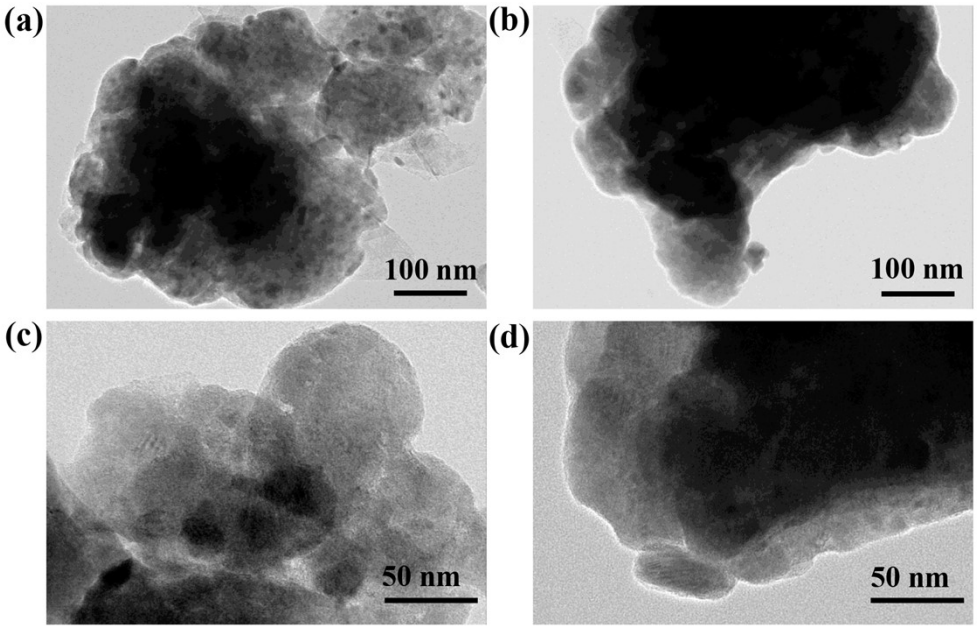

Fig. S7 TEM images of FSS/G-15% in different regions.

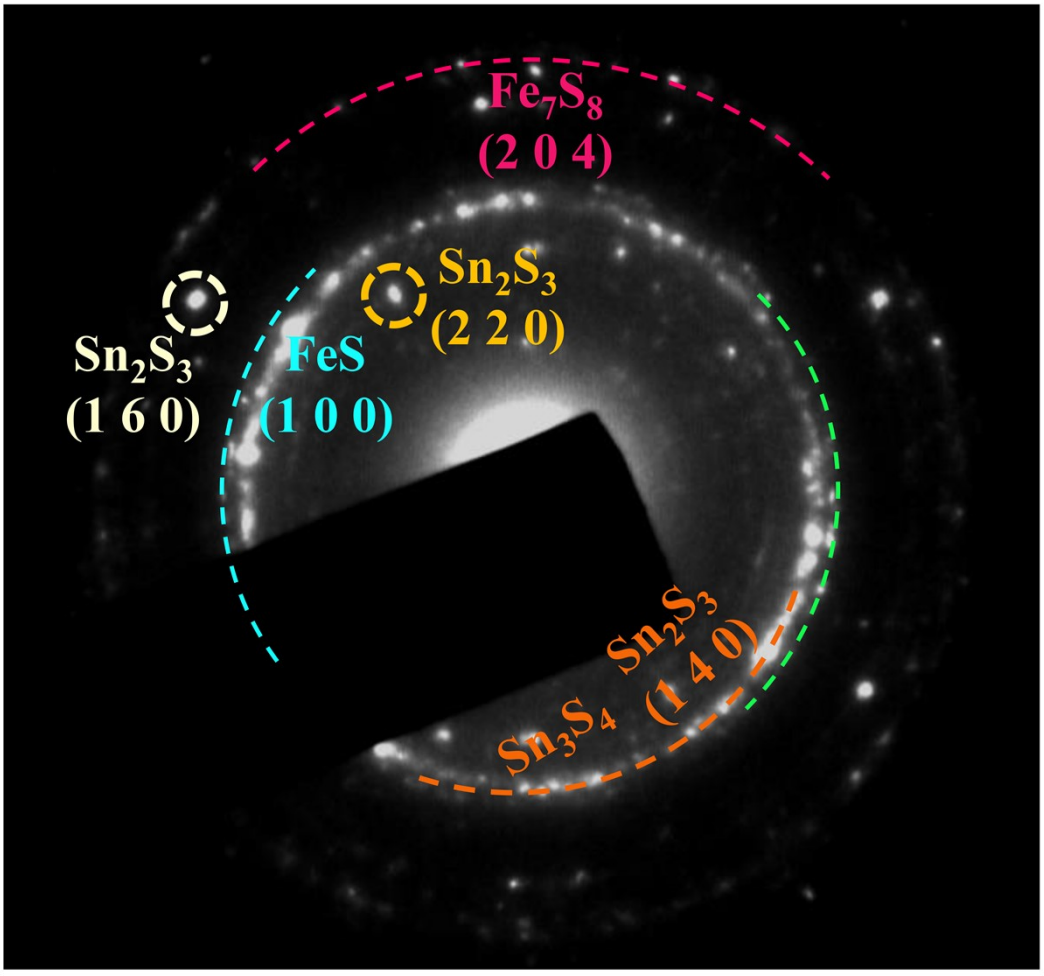

Fig. S8 SAED image of FSS/G-15%.

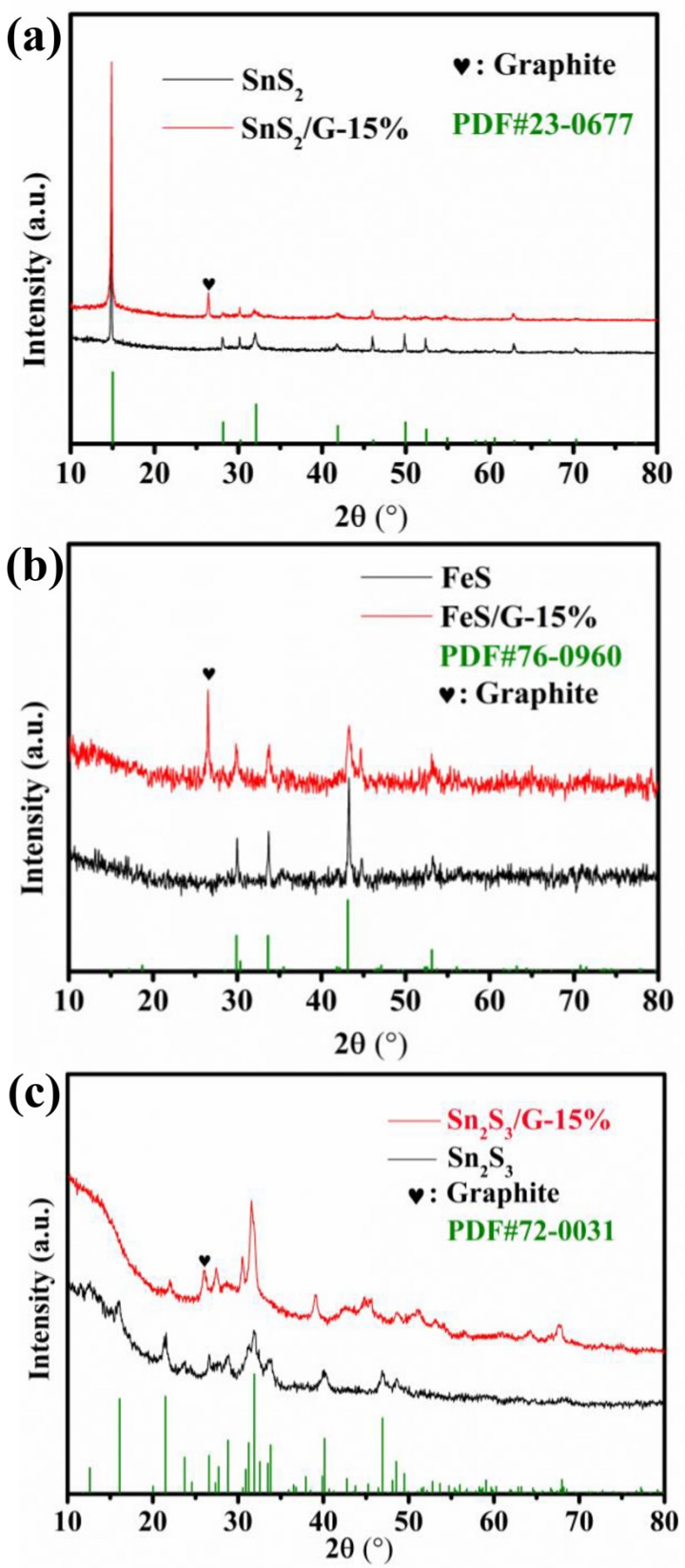

Fig. S9 XRD curves of SnS_2 and SnS_2/G-15% (a), FeS and FeS/G-15% (b), Sn_2S_3 and Sn_2S_3/G-15% (c).

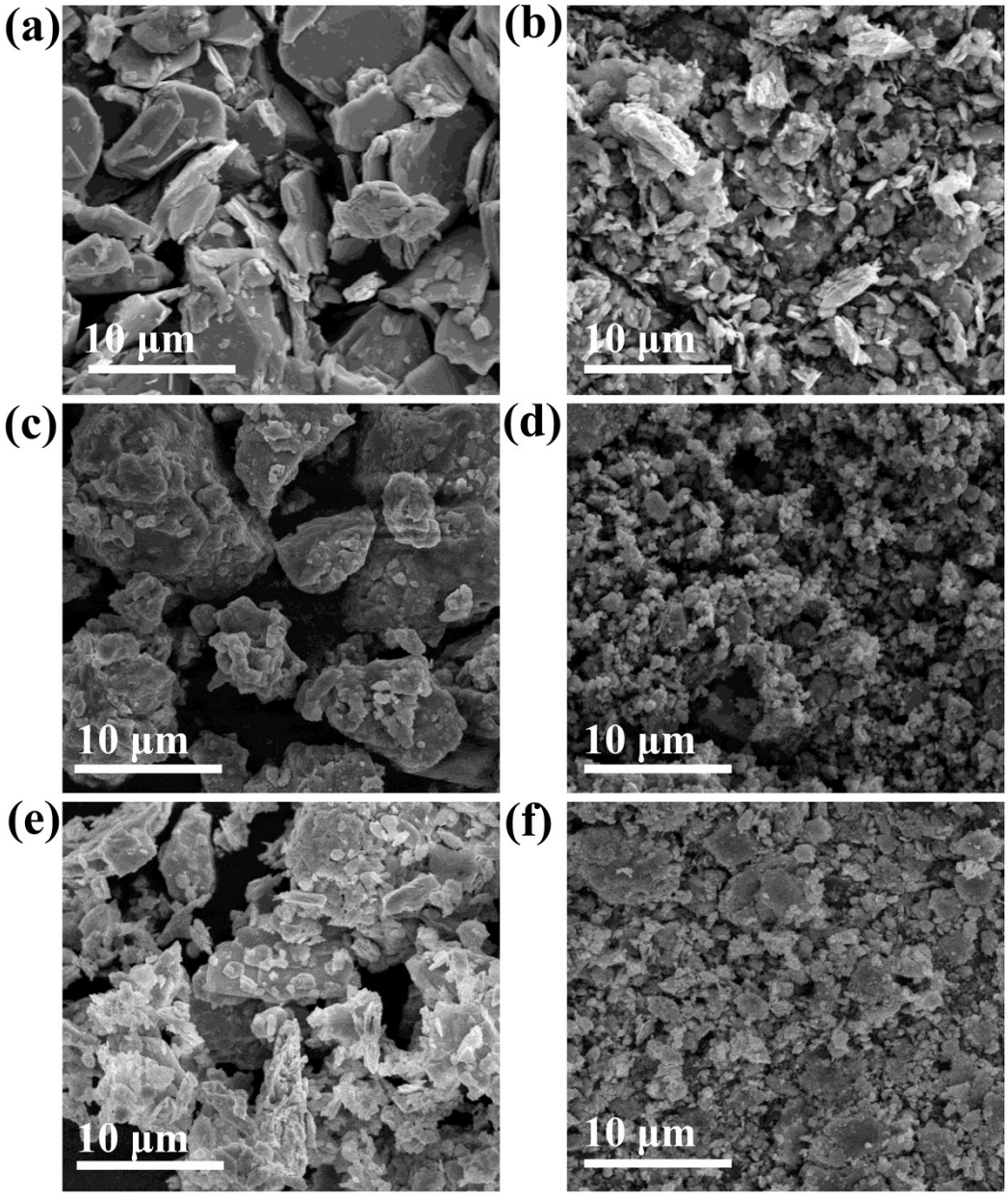

Fig. S10 SEM images of (a) SnS_2 and (b) SnS_2/G-15%, (c) FeS and (d) FeS/G-15%, (e) Sn_2S_3 and (f) Sn_2S_3/G-15%.

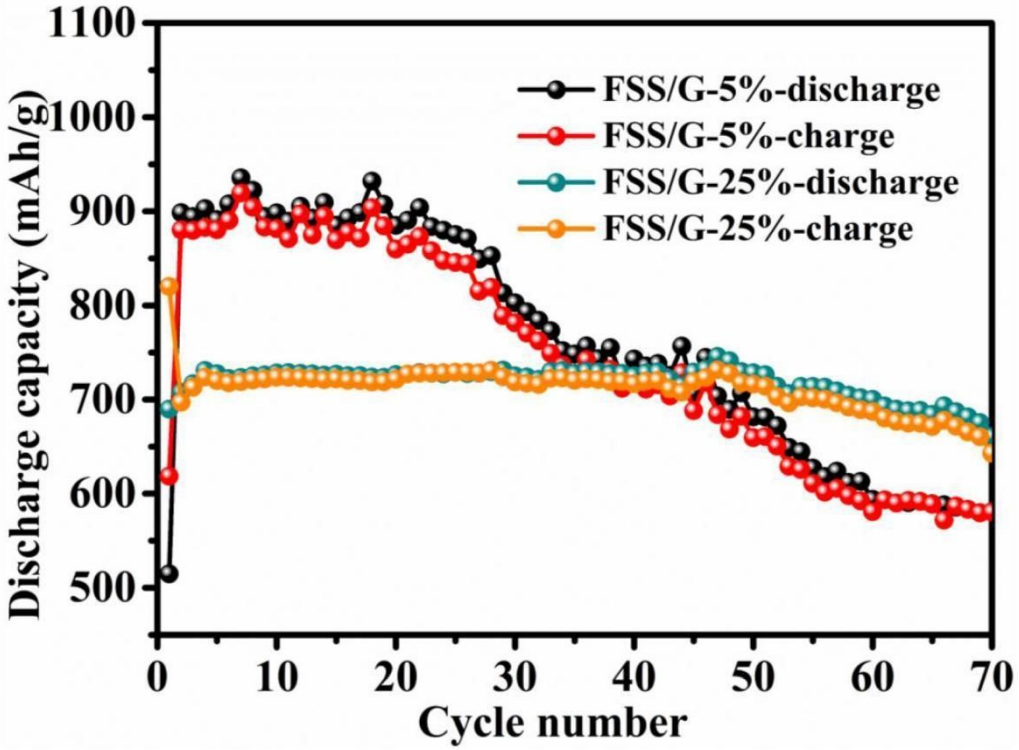

Fig. S11 Cycling performance of FSS/G-5% and FSS/G-25% at 0.1 A g^{-1}.

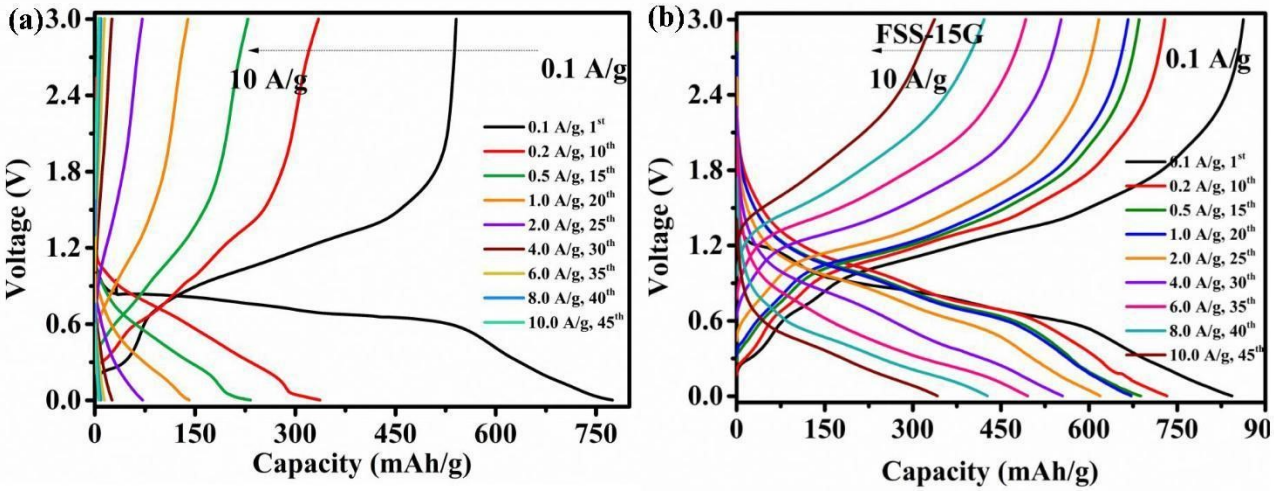

Fig. S12 Discharge/charge curves of FSS (a) and FSS/G-15% (b) from 0.1 to 10 A g^{-1}.

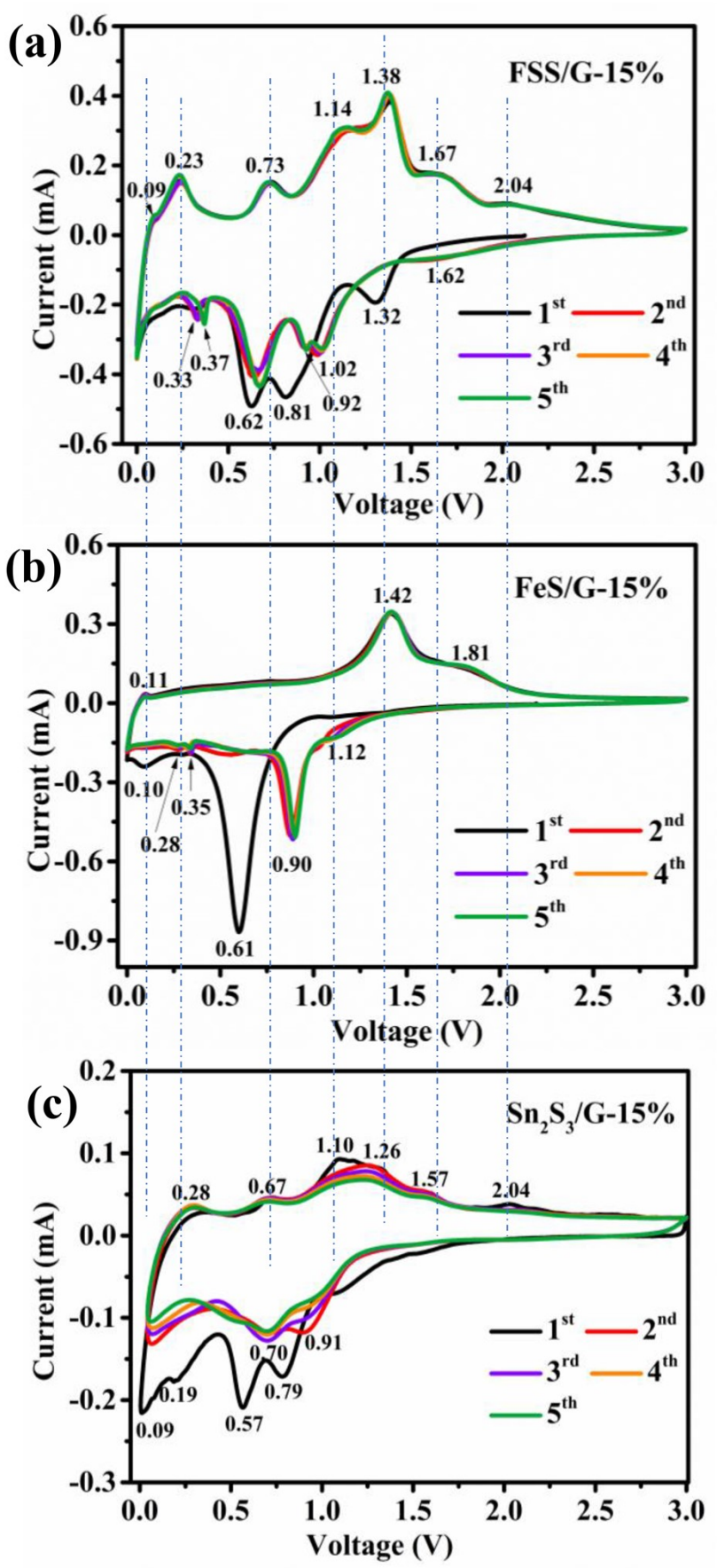

Fig. S13 (a) CV curves of FSS/G-15%, (b) CV curves of FeS/G-15%, (c) CV curves of Sn_2S_3/G-15%.

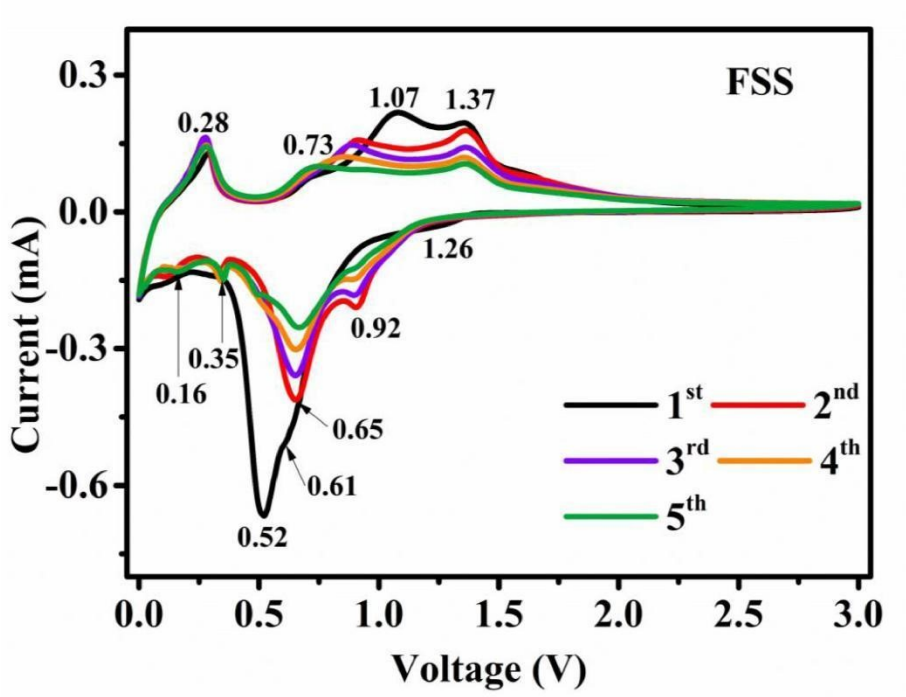

Fig. S14 CV curves of FSS under the scan rate of 0.1 mV s^{-1}.

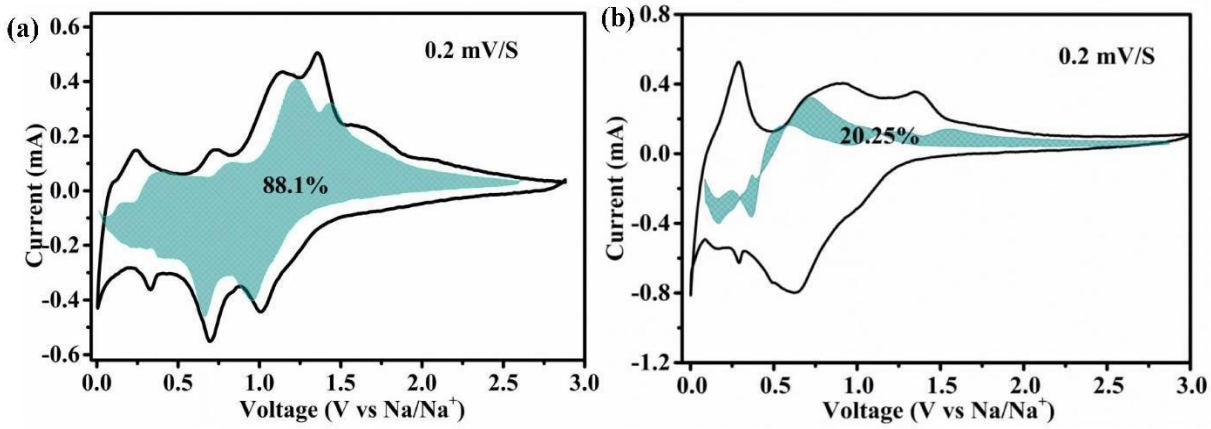

Fig. S15 The pseudocapacitance contributed capacity at 0.2 mV s^{-1} of FSS/G-15% (a) and FSS (b).

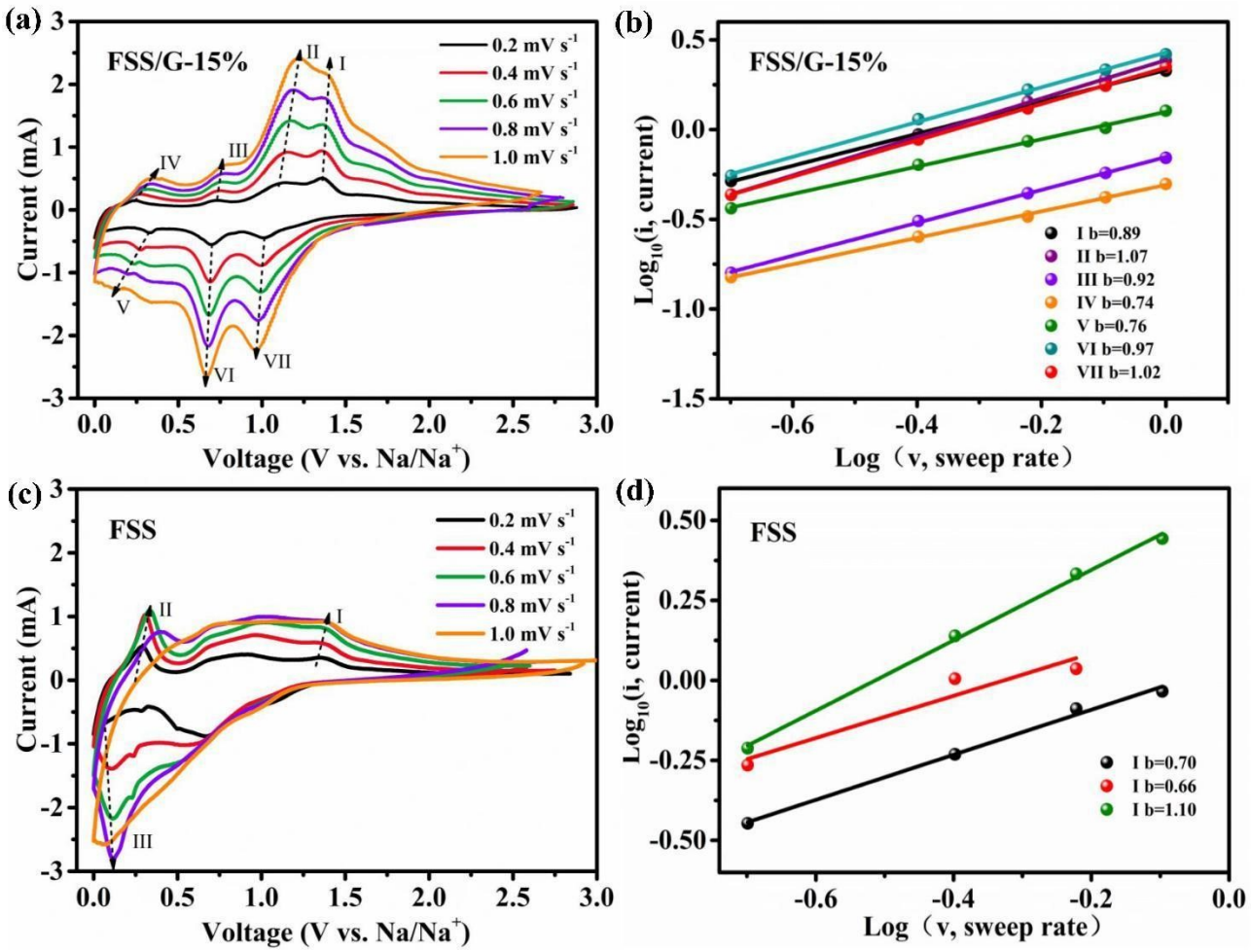

Fig. S16 (a) CV curves of FSS/G-15% under the scan rate of 0.2, 0.4, 0.6, 0.8, and 1.0 mV s^{-1}, (b) $\log_{10}(i)$ against $\log_{10}(v)$ of CV curves of FSS/G-15%, (c) CV curves of FSS under the scan rate of 0.2, 0.4, 0.6, 0.8 and 1.0 mV s^{-1}, (d) $\log_{10}(i)$ against $\log_{10}(v)$ of CV curves of FSS.

The structure of the battery was very similar to the double-layer capacitor, thus the capacities can be divided into diffusion-controlled capacity and pseudo-capacitive capacity. According to B.E. Conway's theory, diffusion-controlled capacity and pseudo-capacitive capacity can be calculated by the following equations[14-16]:

$$i = av^b$$

$$\log_{10}(i) = b\log_{10}(v) + \log_{10}(a)$$

$$i = k_1 v + k_2 v^{1/2}$$

where *a* and *b* are empirical parameters, *v* is the voltage, *i* is the current, k_1 and k_2 are the proportion of the current from surface capacitance and diffusion contributions. The *b* values of FSS and FSS/G-15% were calculated and shown in Fig. S16b, e. The surface capacitance of FSS/G-15% was calculated and shown in Fig. S16c. The *b* values of FSS/G-15% were higher than that of FSS, and the surface capacitance of FSS/G-15% at 1.0 mV s^{-1} reached 96%, illustrating the ultra-fast Na^+ diffuse in FSS/G-15%.

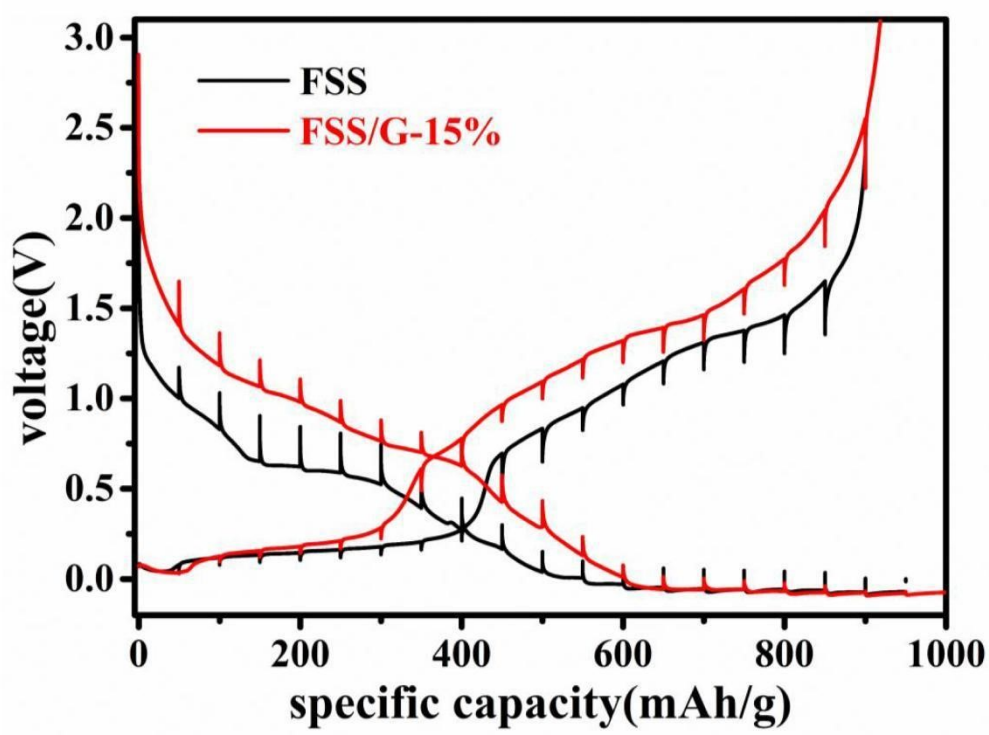

Fig. S17 GITT curves under 0.1 A g^{-1} of FSS/G-15% and FSS after the batteries have undergone 2 discharge/charge cycles.

The D_{Na+} values can be calculated by following equation[17, 18]:

$$D_{Na^+} = \frac{4}{\pi\tau}\left(\frac{m_B \cdot V_B}{M_B \cdot S}\right)\left(\frac{\Delta E_S}{\Delta E_\tau}\right)^2$$

Where m_B is the mass loading (g), M_B is the molecular weight (g mol^{-1}), V_B is the molar volume (cm^3 mol^{-1}), *S* is the contact surface area between the active materials loaded in electrodes (cm^2) and τ is the time of

the current pulse (s). Herein, m_B is based on the FSS content in electrodes, M_B and V_B are based on the 1:2:4 mole ratio of Fe/Sn/S in FSS, S is 1.1310 cm^2, τ is 3600 s.

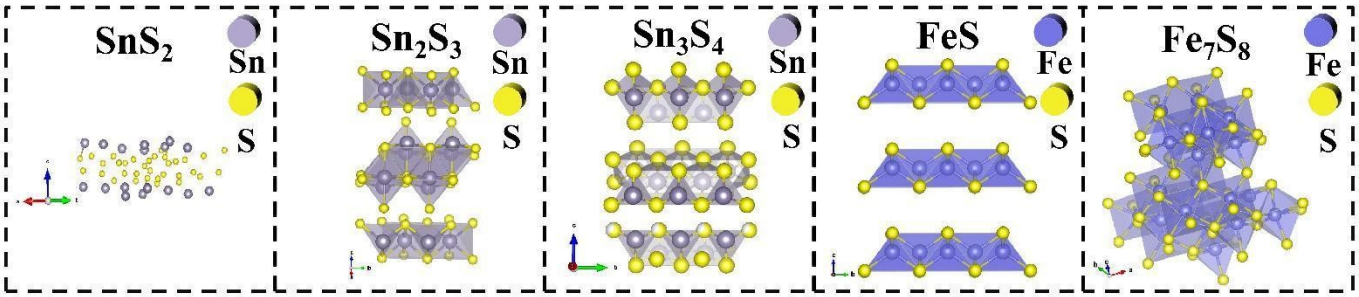

Fig. S18 The crystal models of SnS_2, Sn_2S_3, Sn_3S_4, FeS, and Fe_7S_8 for band structure and band gap calculation.

Table S1 The atomic number and crystal cell parameters of SnS_2, Sn_2S_3, Sn_3S_4, FeS, and Fe_7S_8 for band structure and band gap calculation.

Materials	**Sn**	**Fe**	**S**	**a (Å)**	**b (Å)**	**c (Å)**	**V (Å^3)**
SnS_2	**16**	**0**	**32**	**14.79**	**14.79**	**6.97**	**1323.63**
Sn_2S_3	**16**	**0**	**24**	**9.27**	**7.60**	**14.43**	**1017.26**
Sn_3S_4	**16**	**0**	**22**	**9.91**	**8.12**	**15.42**	**1243.34**
FeS	**0**	**16**	**16**	**7.19**	**7.19**	**10.90**	**564.12**
Fe_7S_8	**0**	**21**	**24**	**6.64**	**6.64**	**15.77**	**603.18**

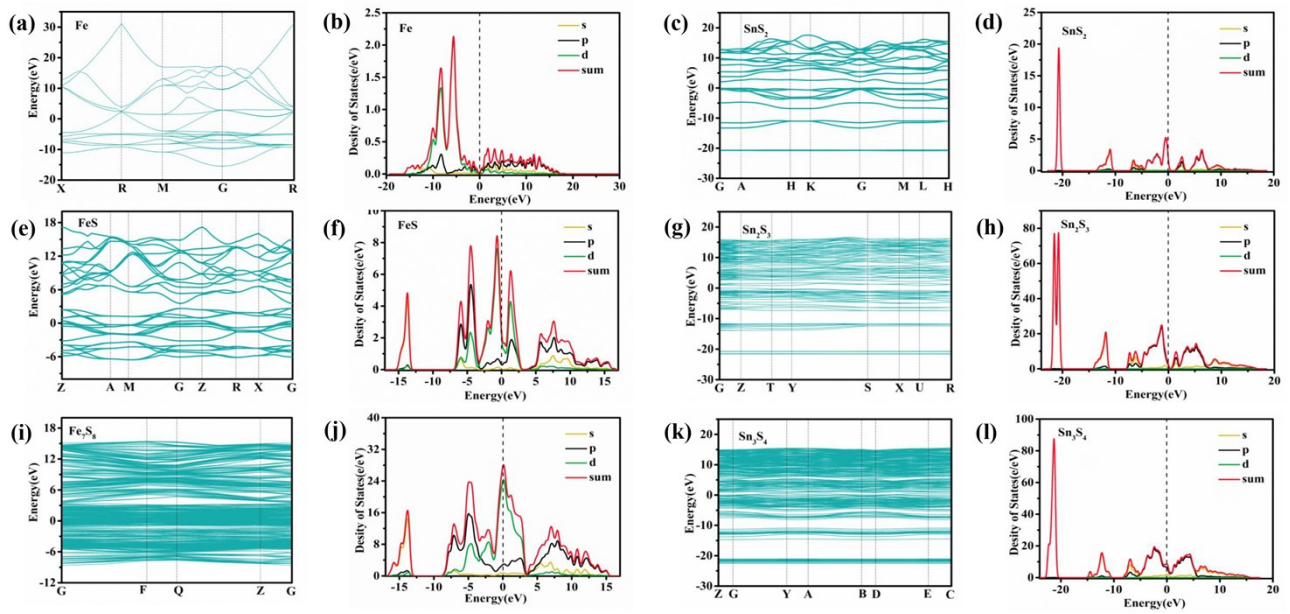

Fig. S19 (a) band structure of Fe, (b) density of the state of Fe, (c) band structure of SnS_2, (d) density of the state of SnS_2, (e) band structure of FeS, (f) density of the state of FeS, (g) band structure of Sn_2S_3, (h) density of the state of Sn_2S_3, (i) band structure of Fe_7S_8, (j) density of the state of Fe_7S_8, (k) band structure of Sn_2S_3, (l) density of the state of Sn_2S_3.

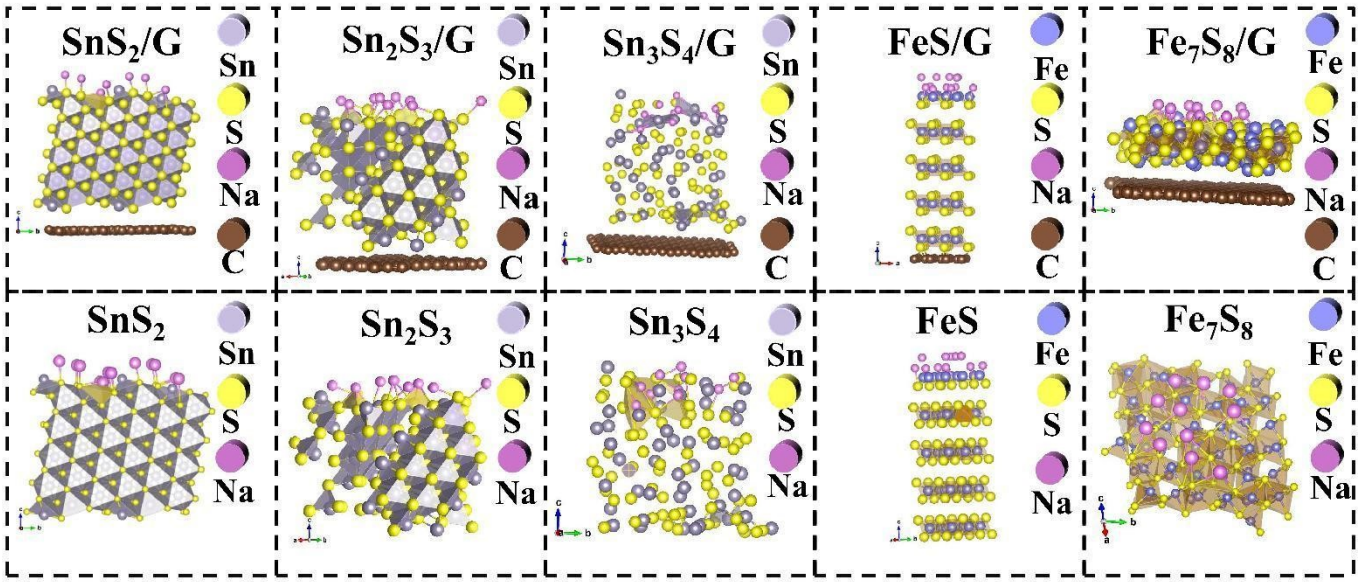

Fig. S20 The crystal models of SnS_2/G, Sn_2S_3/G, Sn_3S_4/G, FeS/G, Fe_7S_8/G, SnS_2, Sn_2S_3, Sn_3S_4, FeS, Fe_7S_8 for MD simulation.

Table S2 The slope of mean square displacement of MD simulation.

Materials	SnS_2	Sn_2S_3	Sn_3S_4	FeS	Fe_7S_8	SnS_2/G	Sn_2S_3/G	Sn_3S_4/G	FeS/G	Fe_7S_8/G
Slope ($\times 10^{-3}$ $Å^3$ ps^{-1})	1.55	0.851	1.71	0.0247	0.0374	2.69	3.1	2.17	0.523	0.0491

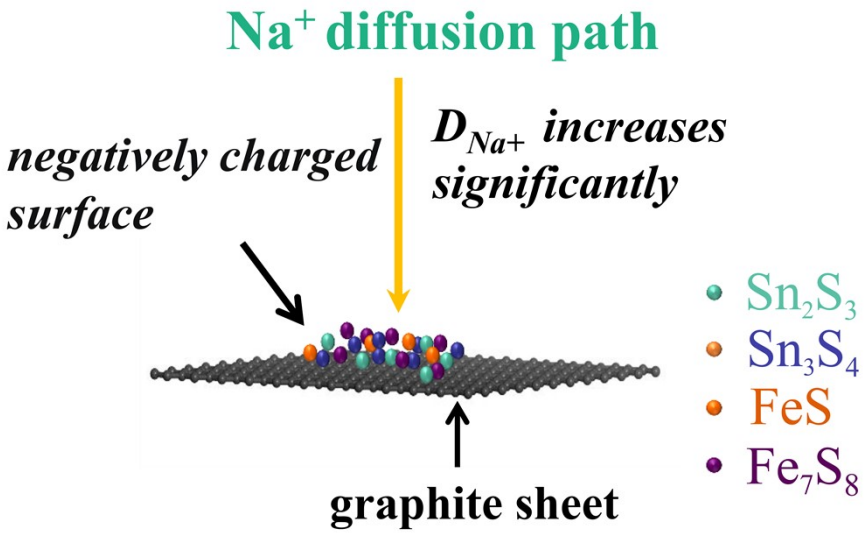

Fig. 21 The schematic of the Na^+ diffuse accelerated by exfoliated graphite.

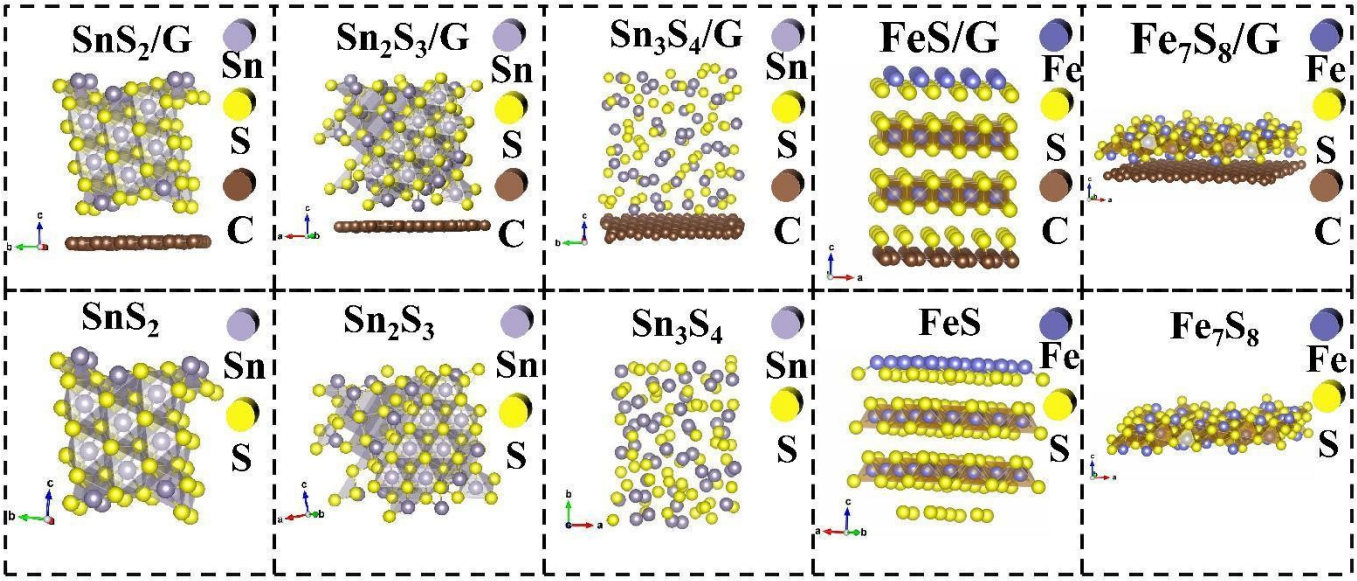

Fig. S22 The crystal models of SnS_2/G, Sn_2S_3/G, Sn_3S_4/G, FeS/G, Fe_7S_8/G, SnS_2, Sn_2S_3, Sn_3S_4, FeS, Fe_7S_8 for work function calculation.

Table S3 The atomic number, crystal cell parameters, Fermi level, vacuum energy level, and work function of the SnS_2, Sn_2S_3, Sn_3S_4, FeS, Fe_7S_8, SnS_2/G, Sn_2S_3/G, Sn_3S_4/G, FeS/G, Fe_7S_8/G.

Materials	Sn	Fe	S	C	a (Å)	b (Å)	c (Å)	V (Å^3)	E-fermi (eV)	E-vacuum (eV)	Ewk (eV)
SnS_2	20	/	40	/	13.34	19.18	36.02	9216.12	-2.73	3.59	6.32
SnS_2/G	20	/	40	48	13.34	19.18	36.02	9216.12	-0.86	4.12	4.98
Sn_2S_3	42	/	62	/	11.99	14.92	36.25	6401.27	-0.89	5.43	6.32
Sn_2S_3/G	42	/	62	73	11.99	14.92	36.25	6401.27	0.39	4.43	3.95
Sn_3S_4	46	/	64	/	14.43	18.92	37.76	10316.78	-0.98	3.97	4.95
Sn_3S_4/G	46	/	64	156	14.43	18.92	37.76	10316.78	-2.61	2.27	4.88
FeS/G	/	48	48	32	18.05	7.19	36.29	4711.64	2.07	4.29	2.22
FeS	/	48	48	/	18.05	7.19	36.29	4711.64	-0.66	6.91	7.57
Fe_7S_8/G	/	45	51	63	23.95	17.11	19.54	7720.72	0.49	4.87	4.38
Fe_7S_8	/	45	51	63	23.95	17.11	19.54	7720.72	-0.81	4.12	4.93

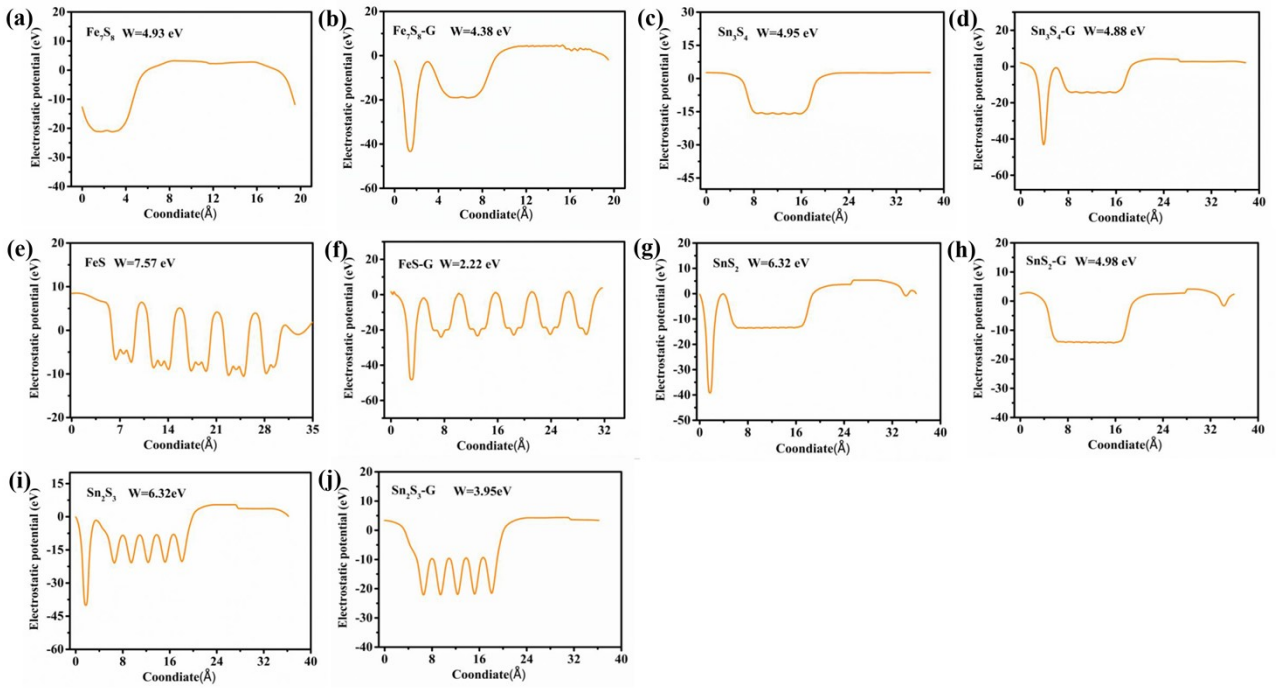

Fig. 23 The electronic escape work functions. (a) Fe_7S_8, (b) Fe_7S_8/G, (c) Sn_3S_4, (d) Sn_3S_4/G, (e) FeS, (f) FeS/G, (g) SnS_2, (h) FeS_2/G, (i) Sn_2S_3, (j) Sn_2S_3/G.

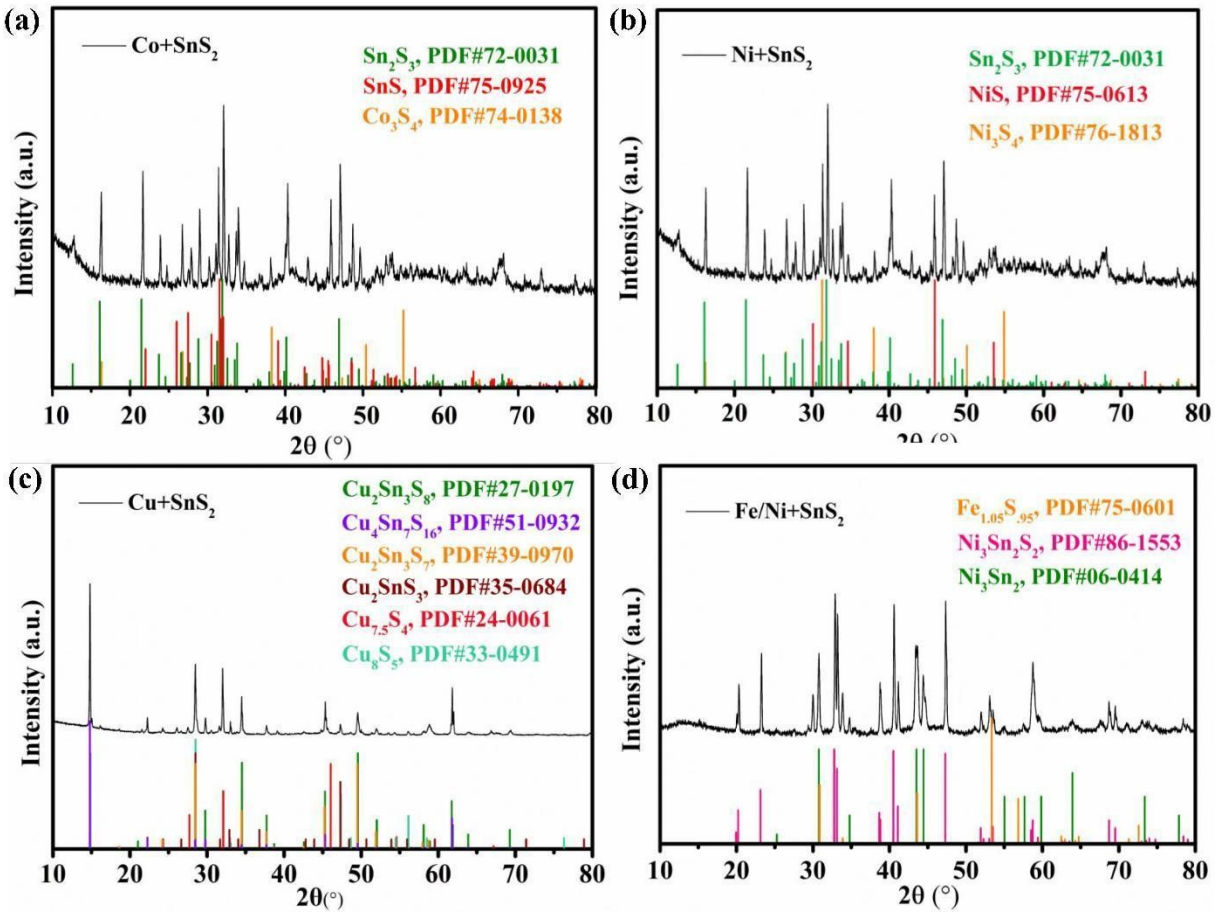

Fig. S24 XRD curves of the products of heated transition metals with SnS_2. (a) Co+SnS_2, (b) Ni+SnS_2, (c) Fe/Ni+SnS_2, (d) Cu+SnS_2.

1. S. G. Charati and S. A. Stern, *Macromolecules*, 1998, **31**, 5529-5535.
2. G. Smirnov, *Physical Review B*, 2020, **102**.
3. S. G. Lewis, D. Ghosh, K. L. Jensen, D. Finkenstadt, A. Shabaev, S. G. Lambrakos, F. Liu, W. Nie, J. C. Blancon, L. Zhou, J. J. Crochet, N. Moody, A. D. Mohite, S. Tretiak and A. J. Neukirch, *J Phys Chem Lett*, 2021, **12**, 6269-6276.
4. M. Xue, J. Xie, W. Li, C. Yang, Y. Ai, F. Wang, J. Ou and J. Yao, *Physica B: Condensed Matter*, 2011, **406**, 4240-4244.
5. C. Fotea, J. Callaway and M. R. Alexander, *Surface and Interface Analysis*, 2006, **38**, 1363-1371.
6. Q. Hong, C. Liu, Z. Wang, R. Li, X. Liang, Y. Wang, Y. Zhang, Z. Song, Z. Xiao, T. Cui, B. Heng, B. Xu, F. Qi and A. Ikhlaq, *Chemical Engineering Journal*, 2021, **417**.
7. T. Wang, W. Lv, D. Meng, Q. Liu, Z. Rong and H. Qiu, *Journal of Alloys and Compounds*, 2022, **925**.
8. W. M. Skinner, H. W. Nesbitt and A. R. Pratt, *Geochimica et Cosmochimica Acta*, 2004, **68**, 2259-2263.
9. H. Wu, L. Li, K. Chang, K. Du, C. Shen, S. Zhou, G. Sheng, W. Linghu, T. Hayat and X. Guo, *Journal of Environmental Chemical Engineering*, 2020, **8**.
10. G. Matyszczak, A. Fidler, E. Polesiak, M. Sobieska, K. Morawiec, W. Zajkowska, K. Lawniczak-Jablonska and P. Kuzmiuk, *Ultrason Sonochem*, 2020, **68**, 105186.

11. Wenping, Xianhong, Yang, Ziqi, Bing, Zhang, Wenyu, Zong, Madhavi and Srinivasan.
12. D. Avellaneda, I. Sánchez-Orozco, J. A. A. Martínez, S. Shaji and B. Krishnan, *Materials Research Express*, 2018, **6**.
13. P. K. Nair, M. Nair, R. A. Zingaro and E. A. Meyers, *Thin Solid Films*, 1994, **239**, 85-92.
14. J. Wojtowicz, N. Marincic and B. E. Conway, *The Journal of Chemical Physics*, 1968, **48**, 4333-4345.
15. J. Wojtowicz and B. E. Conway, *The Journal of Chemical Physics*, 1970, **52**, 1407-1415.
16. C. Chen, Y. Wen, X. Hu, X. Ji, M. Yan, L. Mai, P. Hu, B. Shan and Y. Huang, *Nat Commun*, 2015, **6**, 6929.
17. K. Ise, S. Morimoto, Y. Harada and N. Takami, *Solid State Ionics*, 2018, **320**, 7-15.
18. W. Weppner and R. A. Huggins, *Journal of The Electrochemical Society*, 1977, **124**, 1569.